Journal of Asian Ceramic Societies

ISSN: 2187-0764 (Online) Journal homepage: www.tandfonline.com/journals/tace20

High-temperature properties and thermal stability of monophasic Al_3BC_3

Ryosuke Maki, Shunta Matsumura, Kenta Fukamachi, Eri Takahashi, Ayumi Hayashi, Satofumi Maruyama, Toshiyuki Nishimura, Tomoyuki Maeda, Hatsuo Taira & Yoshihiro Kusano

To cite this article: Ryosuke Maki, Shunta Matsumura, Kenta Fukamachi, Eri Takahashi, Ayumi Hayashi, Satofumi Maruyama, Toshiyuki Nishimura, Tomoyuki Maeda, Hatsuo Taira & Yoshihiro Kusano (2026) High-temperature properties and thermal stability of monophasic Al_3BC_3, Journal of Asian Ceramic Societies, 14:1, 33-41, DOI: 10.1080/21870764.2025.2595816

To link to this article: https://doi.org/10.1080/21870764.2025.2595816

JOURNAL OF ASIAN CERAMIC SOCIETIES
2026, VOL. 14, NO. 1, 33–41
https://doi.org/10.1080/21870764.2025.2595816

THE CERAMIC SOCIETY OF JAPAN
THE KOREAN CERAMIC SOCIETY
Taylor & Francis
Taylor & Francis Group

RESEARCH ARTICLE

OPEN ACCESS Check for updates

High-temperature properties and thermal stability of monophasic Al_3BC_3

Ryosuke Maki[a], Shunta Matsumura[a], Kenta Fukamachi[a], Eri Takahashi[b], Ayumi Hayashi[b], Satofumi Maruyama[b], Toshiyuki Nishimura[c], Tomoyuki Maeda[d], Hatsuo Taira[d] and Yoshihiro Kusano[a]

[a]Department of Applied Chemistry, Okayama University of Science, Kita-ku, Okayama, Japan; [b]Department of Mechanical Engineering, Tokyo City University, Setagaya, Tokyo, Japan; [c]Research center for structural materials, National Institute for Materials Science, Tsukuba, Ibaraki, Japan; [d]Okayama Ceramics Research Foundation, Bizen, Okayama, Japan

ABSTRACT

This paper describes the detailed high-temperature properties of monophasic Al_3BC_3, including the thermal expansion characteristics of its crystal structure and thermal shock resistance. We examined the differences in physical properties between Al_3BC_3 and $Al_8B_4C_7$, which was previously thought to be Al_3BC_3. Compared with the thermal conductivity and CTE of Al_3BC_3 measured in the present study, those reported for $Al_8B_4C_7$ in a previous study were higher, which is attributable to residues of Al and B. The densification of $Al_8B_4C_7$ is supported by gas-phase diffusion via Al- and B-based gases or liquid, whereas the sintering of Al_3BC_3 is dominated by solid-phase diffusion. The bending strength of Al_3BC_3 was 226 MPa at RT and was maintained even at high temperatures. Al_3BC_3 was found to exhibit a good thermal shock fracture resistance parameter R' of 3.3, equivalent to that of Al_2O_3 and substantially better than that of commonly used engineering ceramics Al_4SiC_4 and $Al_6Si_2O_{13}$, mainly because of the higher thermal conductivity and lower elastic modulus of Al_3BC_3. The dense Al_3BC_3 sample exhibited excellent thermal stability under N_2 and inert gas atmospheres but was easily oxidized to monophasic Al_2O_3 at 1300°C under ambient air.

ARTICLE HISTORY
Received 31 May 2025
Accepted 23 November 2025

KEYWORDS
Ternary metal borocarbide (Al_3BC_3); refractory; thermal properties; mechanical properties; thermal stability

1. Introduction

Ternary aluminum borocarbide, Al_3BC_3, is a promising candidate for use in lightweight structural components and is an important sintering additive for ultrahigh-temperature structural materials such as SiC and ZrB_2 [1,2]. The chemical composition of Al_3BC_3 was previously believed to be $Al_8B_4C_7$ [3–5]; thus, numerous properties of Al- and B-excess samples have been reported. Wang and Yamaguchi [6] prepared a dense sample by heating a powdered mixture of Al, B_4C, and C according to the composition ratio of $Al_8B_4C_7$ using spark plasma sintering (SPS) and measured its thermal and mechanical properties at room temperature (RT). Hashimoto *et al*. [1] reported that dense $Al_8B_4C_7$ exhibits an excellent bending strength of ~510 MPa at high temperatures and is thus expected to be useful as a high-temperature construction material. Li *et al*. [7] achieved the synthesis of bulk Al_3BC_3 samples containing a small amount of B_4C and graphite via a reactive hot-pressing method. They reported the RT mechanical properties of as-synthesized Al_3BC_3 and clarified the temperature dependence of the Young's modulus. Recently, a computational approach has been used to predict physical properties based on the crystal structure, and knowledge of the structural parameters at high temperatures is desirable. In a study based on first-principles calculations, Wang *et al*. [8] showed that ternary metal borocarbides (e.g. Al_3BC_3, Sc_2BC_2, and Lu_3BC_3) containing short linear C – B – C units experience low shear-strain resistance and might exhibit damage tolerance.

Crystalline Al_3BC_3 exhibits excellent thermal stability under inert atmospheres and is not sensitive to hydrolysis; however, it is susceptible to oxidation in air at ≥1200°C [9,10]. Thus, the addition of Al_3BC_3 markedly inhibits oxidation, functioning as an antioxidant for composite materials such as carbon-containing refractories (e.g. MgO – C) [11]. Al_3BC_3 decomposes at high temperature to form Al_2O_3, B_2O_3, $Al_{18}B_4O_{33}$, and CO/CO_2. These products create a dense Al-B-O layer and a locally reducing atmosphere, effectively suppressing oxidation of the ceramic components. As structural material, the dense ZrB_2/Al_3BC_3 and $ZrB_2/SiC/Al_3BC_3$ compounds have various excellent properties, including high hardness, high flexural strength, good fracture toughness, and high thermal shock resistance [12,13]. However, the high-temperature properties of monophasic Al_3BC_3 remain unclear. Here, we measured various high-temperature properties of dense Al_3BC_3 single-phase samples and clarified their thermal

CONTACT Yoshihiro Kusano kusano@ous.ac.jp Department of Applied Chemistry, Okayama University of Science, 1-1 Ridai-Cho, Kita-Ku 700-0005, Japan

Supplemental data for this article can be accessed online at https://doi.org/10.1080/21870764.2025.2595816

shock resistance. We also investigated the thermal expansion characteristics and thermal stability of Al_3BC_3 under air, N_2, and inert gas atmospheres.

2. Experimental procedures

2.1. Sample preparation

The starting material Al_3BC_3 was prepared as described in the literature and subsequently pulverized by vibration-milling for 3 min [14]. To prepare a dense sample, Al_3BC_3 powder with a grain size of 1–20 μm was heated under flowing Ar (5 L/min) to 1600°C at a rate of 30°C/min under a uniaxial pressure of 40 MPa by SPS. Only the samples for thermal property measurement were sintered under a uniaxial pressure of 30 MPa. The shrinkage of the samples during SPS was monitored; the samples were maintained at the same temperature until the shrinkage ceased and were then cooled to RT in the furnace.

2.2. Crystallographic analysis

The formed phases were characterized by powder X-ray diffraction (XRD) with Cu-Kα radiation (SmartLab, equipped with a HyPix-3000 two-dimensional semiconductor detector, Rigaku, Japan). The thermal expansion characteristics of the Al_3BC_3 crystal structure were characterized via in situ measurements using high-temperature XRD (HT-XRD); the pulverized Al_3BC_3 sample was placed on an alumina holder covered with a graphite sheet and heated to 1200°C under Ar. The lattice constant was calculated on the basis of Si powder added as an internal standard (SRM640b, NIST, USA). The crystal structure at high temperatures was refined via Rietveld refinement.

2.3. Physical property measurements

The bulk density of the sintered samples was measured by the Archimedes method. The coefficient of linear thermal expansion (CTE) was measured by thermomechanical analysis (DIL402CD, NETZSCH Japan), with the samples heated to 1200°C under Ar. Thermal diffusivity and specific heat were measured in the temperature range 25–1000°C by the laser flash method (LFA-457, NETZSCH Japan) with the sample under Ar; a standard sapphire sample was used as a reference material.

The samples used for bending tests were cut into quadrangular bars with dimensions of $4 \times 3 \times 20\ mm^3$. The bending strength was measured in the temperature range 25–1400°C via a three-point bending test using a universal testing machine (Autograph, Shimadzu) with the sample under Ar; the span was 16 mm, the crosshead speed was 0.5 mm/min, and a SiC jig was used.

2.4. Thermal stability evaluation

The thermal stability of the sintered Al_3BC_3 sample was evaluated by in situ HT-XRD measurements at temperatures as high as 1300°C and 1500°C under N_2 and dry air (78% N_2 and 22% O_2) gas flows (200 mL/min), respectively. Microstructural observation was conducted using scanning electron microscopy (SEM, SU8010, Hitachi) in conjunction with energy-dispersive X-ray spectroscopy (EDS).

3. Results and discussion

3.1. Crystallographic analysis

Figure 1 presents HT-XRD patterns for the Al_3BC_3 powder at different temperatures in the range 29–1200°C. The diffraction peaks in the XRD pattern were attributed to monophasic Al_3BC_3 with a trigonal unit cell ($P\bar{3}c1$), except for peaks from the Si standard and carbon sheet. Al_3BC_3 exhibited excellent thermal stability to 1200°C under inert atmospheres. The diffraction peaks shifted to lower angles with increasing temperature, indicating thermal expansion. Through Rietveld refinement, the lattice constants *a* and *b* of Al_3BC_3 were found to increase linearly (Figure 2 and Table S1). The CTE along the *a*-axis and *c*-axis were determined to be 7.08×10^{-6}/°C and 5.10×10^{-6}/°C, respectively, in the temperature range from 29 to 1200°C. For the *c*-axis, the thermal expansion tendency of the lattice constant varied at 600°C. The linear thermal expansion was most anisotropic when the sample was heated to 500°C: the CTE along the *a*-axis was approximately twice as large as that along the *c*-axis. Several ceramic materials such as karrooite and cordierite are known to cause microcracks inside sintered ceramic bodies because of anisotropic thermal expansion, which adversely affects the mechanical strength [15,16]. The CTE for the Al_3BC_3 crystal structure was relatively small; thus, cracking due to thermal stress is unlikely to occur.

The changes in structural parameters with increasing temperature, as evaluated through Rietveld refinement, are shown in Figure 3. The reliability indices R_{wp} and *S* were in the ranges 6.9–11.9% and 1.0–1.5, respectively. The crystal structure of Al_3BC_3 is believed to be as follows: Isolated C atoms are located at the center of corner-sharing CAl_5 trigonal bipyramids, which are interleaved by short linear C – B – C units containing strong covalent bonding along the *c*-axis. This bonding is commonly described within the $(Al^{3+})_3(C^{4-})(CBC)^{5-}$ ionic formalism; the C – B – C unit can then be interpreted as an anion $(C=B=C)^{5-}$ with 16 valence electrons [4]. At RT, short linear C – B – C units with a C2–B distance of 0.131 nm were located between CAl_3 layers. The distance suddenly expanded to 0.149 nm at 400°C, and this distance was maintained to 1000°C. In the CAl_5 bipyramids, Al atoms were coordinated as slightly

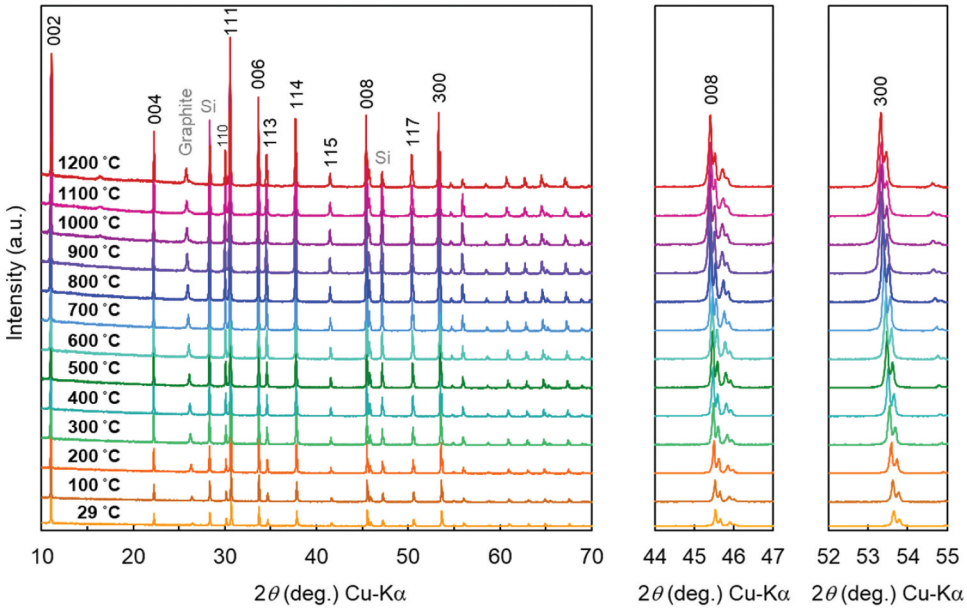

Figure 1. HT-XRD patterns for Al_3BC_3 powder heated at different temperatures under Ar flow.

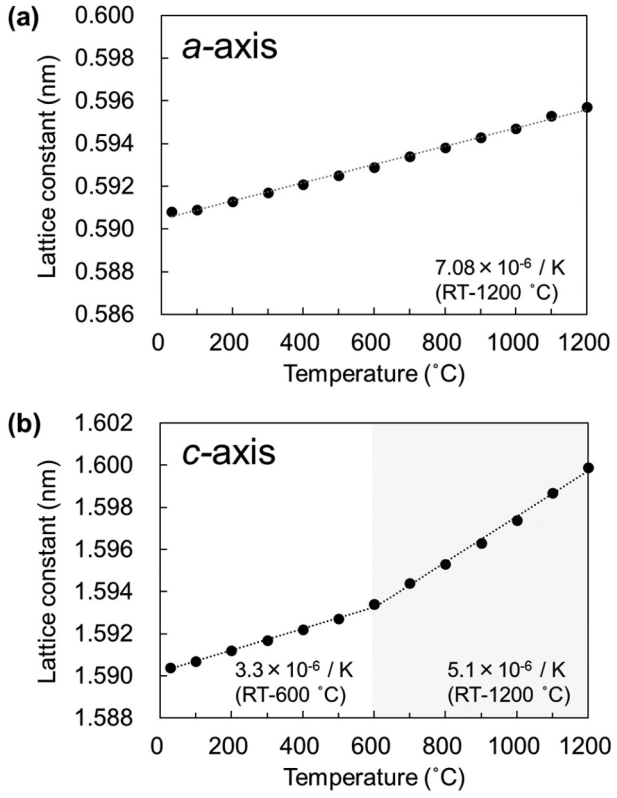

Figure 2. Lattice constants along (a) *a*-axis and (b) *c*-axis for Al_3BC_3 crystal structure with trigonal cell ($P\bar{3}c1$), plotted as functions of heating temperature.

distorted polyhedra with C1–Al2 distances of 0.206 nm (×2), a C1–Al1 distance of 0.182 nm, and a C1–Al3 distances of 0.204 nm (×2) at RT. The C – Al bond length in the CAl_3 layer changed substantially at 600°C. The bond angle (Al2–C1–Al2) also changed according to the change in interatomic distance, causing tetrahedral distortion without a corresponding volume expansion. However, the C1–Al3 bond length began to increase at temperatures greater than 700°C, leading to a change in the thermal expansion tendency of the lattice constant along the *c*-axis at 700–1200°C, as shown in Figure 2. The bond angle (Al3–C1–Al3) changed in accordance with the variation in the interatomic distance of the C – B – C units at 400°C, since the Al3 atom is adjacent to the C2 atom. Upon heating, the C – Al bond length in the CAl_3 layer remained unchanged; however, the displacement of the Al3 atom resulted in an elongation of the C1–Al3 bond length and a concomitant decrease in the Al3–C1–Al3 bond angle. The predominant effect of short linear C – B – C units on mechanical properties is known to lead to a low shear modulus [8]. Shear deformation of Al_3BC_3 is caused by easy tilting of rigid C – B – C units with respect to the *c*-axis and shear sliding of corner-sharing CAl_5 bipyramids. The changes in atomic position and distortion occurring at 400–600°C might adversely affect the deduced properties of Al_3BC_3, such as lowering its shear-strain resistance, which indicates the need for further investigation into the dependence of the mechanical properties of Al_3BC_3 on its crystal orientation at various temperatures.

3.2. Physical property measurements

Figure 4 shows the thermal expansion rate for the sintered Al_3BC_3 sample from the first to the third heating cycle under flowing Ar. The thermal expansion rate in the first cycle was higher than those in the second and third tests, likely because the pressure produced during SPS generated residual stress inside the sintered body, which was then removed by the first heating step. As a result, the CTE for the sintered Al_3BC_3 sample measured from the third heating curve was 6.37×10^{-6}/°C, which was very close to the average value calculated on the basis of the unit-cell

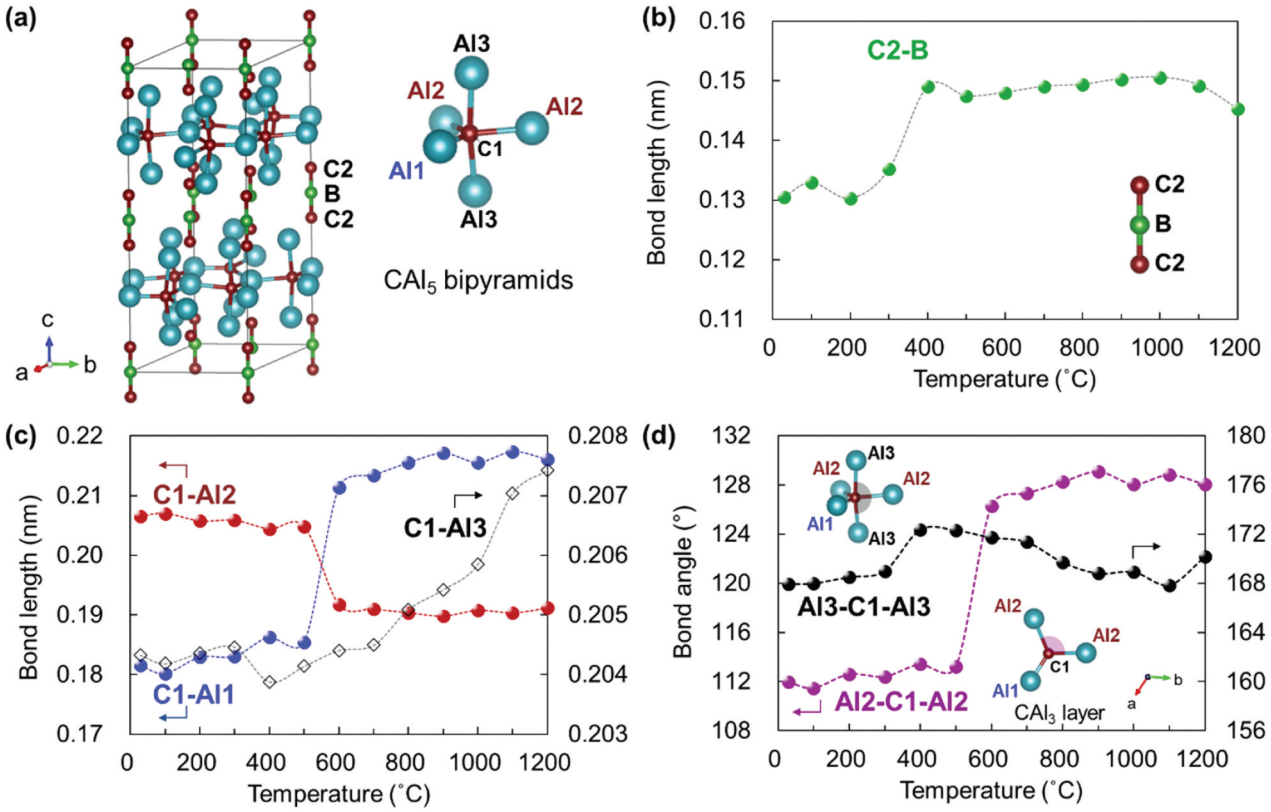

Figure 3. (a) Crystal structure of Al_3BC_3 and CAl_5 trigonal bipyramid. Bond lengths for (b) C2–B and (c) C1–Al1, C1–Al2, and C1–Al3 and (d) bond angle for Al2–C1–Al2 and Al3–C1–Al3 as functions of heating temperature. The crystal-structure model in (a) was illustrated using VESTA [17].

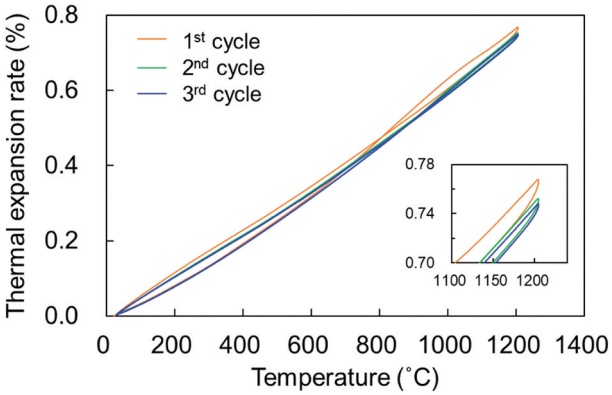

Figure 4. Thermal expansion rate for sintered Al_3BC_3 sample during first to third heating cycle under flowing Ar.

parameters measured by HT-XRD in the temperature range RT–1200°C. The thermal expansion coefficient for Al_3BC_3 was similar to those for Al_4SiC_4 and mullite ($Al_6Si_2O_{13}$).

The thermal diffusivity, heat capacity, and thermal conductivity of the sintered Al_3BC_3 sample are presented in Figure 5. The thermal diffusivity decreased with increasing temperature from 8.7 to 2.0 mm^2/s at 1000°C because of phonon scattering. The specific heat capacity increased as the temperature rose, reaching its maximum at 800°C, ranging from 0.9 to 1.4 J/(g·K). The thermal conductivity was corrected for the porosity of the sintered sample. The porosity was calculated on the basis of the theoretical density, k_0, via the following equation:

$$\kappa = \kappa_0(1 - P)$$

where k and P are the measured thermal conductivity and the porosity, respectively [18]. The thermal conductivity of the sintered Al_3BC_3 sample was 20.94 W/(m·K) at RT and 7.35 W/(m·K) at 1000°C, similar to that of Al_2O_3 at high temperatures. Compared with the thermal conductivity and CTE obtained for Al_3BC_3 in the present study, those previously reported by Wang and Yamaguchi [6] for $Al_8B_4C_7$ (29.2 W/(m·K) and 6.67×10^{-6}/°C) were higher, possibly because of residues of Al and B.

The relative density of the sintered Al_3BC_3 samples prepared for strength measurement was over 96%. Figure 6 presents the bending strength measured at different temperatures under flowing Ar. The bending strength was 226 MPa at RT and increased to 273 MPa at 400°C. This increase in strength is speculatively attributed to micropores and cracks being closed at high temperatures by the thermal expansion of the crystalline particles (Figure 2). The sample then maintained the strength as the temperature was increased. Even at a high temperature of 1400°C, the Al_3BC_3 sample exhibited nearly the same strength as at RT. The strength exceeded the value of previously reported Al_3BC_3 [7]. On the other hands, the strength

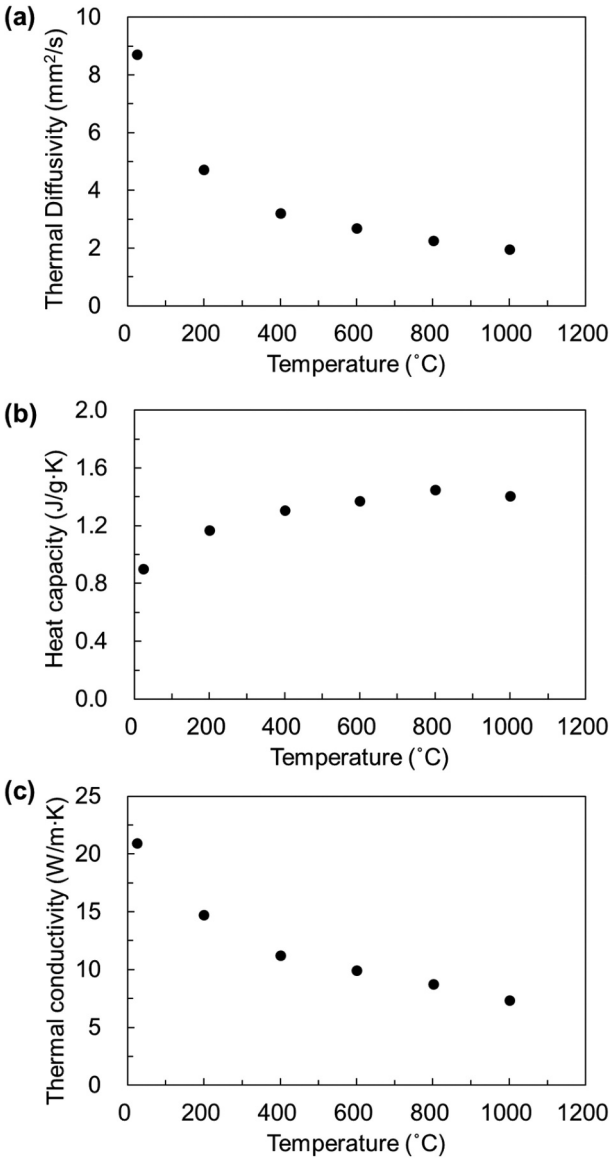

Figure 5. (a) Thermal diffusivity, (b) heat capacity, and (c) thermal conductivity of sintered Al_3BC_3 sample. The thermal conductivity was corrected for porosity.

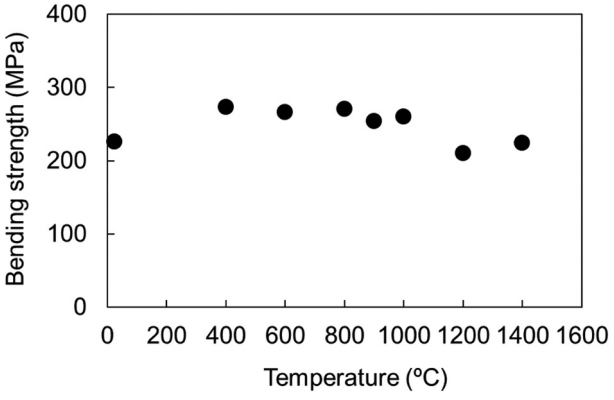

Figure 6. Bending strength of sintered Al_3BC_3 samples tested at different temperatures under flowing Ar.

was lower than that of the previously reported $Al_8B_4C_7$ (500 MPa at RT, relative density of 99.6%), which is likely attributable to difficulties in synthesizing a dense Al_3BC_3 sample although the sintering temperature (1600 °C) was close to its decomposition temperature under SPS conditions (1630°C). According to the results of Wang and Yamaguchi [9], gas-phase diffusion via Al and B gases is believed to be one of the predominant mass transfer mechanisms. Solid-phase diffusion is much slower than the process that involves gas or liquid; thus, the densification of monophasic Al_3BC_3 was likely not completed by SPS in the present study. In the XRD pattern of $Al_8B_4C_7$ reported previously, no peaks attributed to impurity phases were found. In samples synthesized with the nominal composition of $Al_8B_4C_7$, it is likely that excess Al and B are distributed at the grain boundaries, which affect the strength of Al_3BC_3 where intergranular fracturing occurs. In contrast, in the present study, the starting composition was adjusted to the stoichiometric ratio of Al_3BC_3, and the Rietveld refinement concluded that the Al_3BC_3 phase has a stoichiometric composition. Thus, we consider that there is no excess Al or B at the grain boundaries in our synthesized Al_3BC_3 samples. In other words, adding an appropriate amount of Al or B would promote densification and further improve strength.

Figure 7 shows the deformation curves of sintered Al_3BC_3 samples measured at different temperatures. Al_3BC_3 sample exhibited elastic deformation, where the stress increased linearly up to the maximum point. The distortion also became larger as the micropores and cracks closed due to the thermal expansion from RT to 400°C. After that, the strain of the sample decreased with increasing temperature from 400 to 1200°C.

Table 1 shows a summary of the thermal and mechanical properties of the sintered Al_3BC_3 sample. The materials used for comparison are Al_4SiC_4, which is also a promising additive for SiC, and the commonly used engineering ceramics Al_2O_3 and $Al_6Si_2O_{13}$. The CTE and thermal conductivity for Al_3BC_3 are relatively low and very high, respectively, compared with those of Al_4SiC_4 and $Al_6Si_2O_{13}$. In terms of mechanical

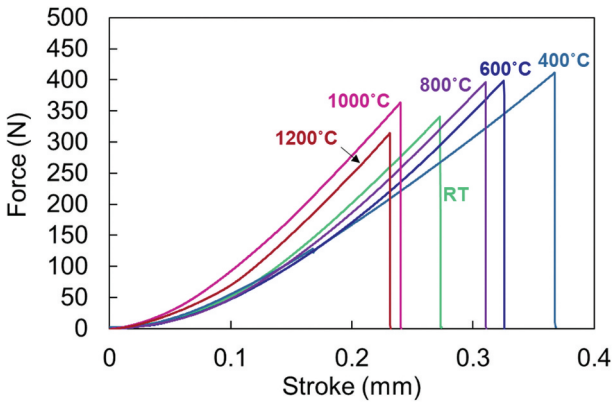

Figure 7. Deformation curves of sintered Al_3BC_3 samples measured from the three-point bending test at different temperatures.

Table 1. Thermal and mechanical properties of sintered Al_3BC_3 sample and various comparison materials.

Sample	Al_3BC_3 (This research)	Al_4SiC_4 [19–22]	Al_2O_3 [21]	$Al_6Si_2O_{13}$ [23–27]
Theoretical density (g/cm^3)	2.66	3.03	3.95	3.12
CTE ($\times10^{-6}$/°C)	6.4 (~1200 °C)	7.2 (~1200 °C)	8.5 (~1000 °C)	5.5 (~1000 °C)
Thermal conductivity (W/m·K)	20 (RT)	7.8 (RT)	32 (RT)	5.1 (RT)
Bending strength (MPa)	226 (RT) 210 (1400°C)	301 (RT) 282 (1400°C)	350 (RT) 130 (1500°C)	255 (RT)
Elastic modulus (GPa)	163 [7]	192	406	174
Poisson's ratio	0.28 [7]	0.21	0.21	0.24
Thermal shock fracture resistance parameter R'	3.3	1.3	2.6	1.0

properties, Al_3BC_3 is a lightweight ceramic with a density of 2.66 g/cm^3; at high temperatures, its strength is similar to that of $Al_6Si_2O_{13}$ but greater than that of Al_2O_3. The elastic modulus reported for Al_3BC_3 is the lowest among these ceramics and is similar to that for cordierite (~140 GPa) [28], which is known as a thermal-shock-resistant material.

To evaluate the thermal stress fracture resistance of monolithic Al_3BC_3, which corresponds to the resistance to crack initiation under thermal stress, we calculated the fracture-resistance parameter R' on the basis of the thermal and mechanical properties via the following equation reported by Hasselman [29]:

$$R' = \frac{\sigma_f \kappa (1-\nu)}{E\alpha}$$

where σ_f is the fracture strength, ν is the Poisson's ratio, E is the Young's modulus of elasticity, and α is the CTE. Herein, the bending strength was used for the calculation. Al_3BC_3 exhibited an excellent R' of 3.3, which is equivalent to that for Al_2O_3 and substantially greater than those for Al_4SiC_4 and $Al_6Si_2O_{13}$, mainly because of the higher thermal conductivity and lower elastic modulus for Al_3BC_3. The calculation results show that no initial cracks occur during thermal shock at $\Delta T \approx 180$°C, thus preserving the strength of the Al_3BC_3.

3.3. Thermal stability evaluation

Figures 8 and 9 present the results of HT-XRD measurements performed at high temperatures under N_2 and dry air atmospheres to evaluate the thermal stability of the sintered Al_3BC_3 samples. AlN has been reported to be formed during heat treatment of Al_3BC_3 powder under an N_2 atmosphere [30]; however, in the present study, the dense Al_3BC_3 sample showed excellent thermal stability and remained monophasic Al_3BC_3 even after the sample was heated under N_2 at 1300°C. By contrast, when Al_3BC_3 was heated in air, small amounts of $Al_{18}B_4O_{33}$ and Al_2O_3 were produced at 1300°C, as described by the following equations:

$$6Al_3BC_3 + 36O_2 \rightarrow Al_{18}B_4O_{33}(s) + B_2O_3(g) + 18CO_2(g)$$

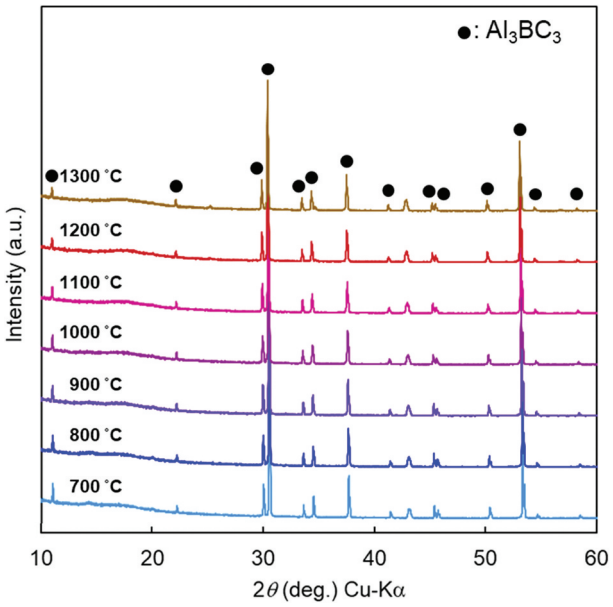

Figure 8. HT-XRD patterns for sintered Al_3BC_3 sample heated at different temperatures under flowing N_2.

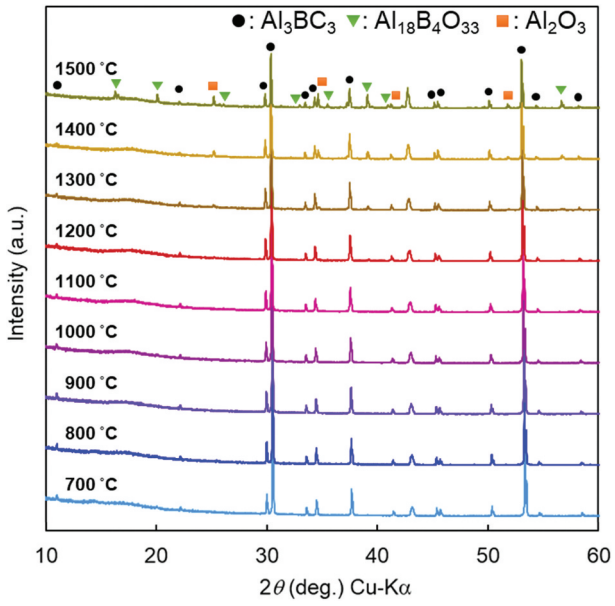

Figure 9. HT-XRD patterns for sintered Al_3BC_3 sample heated at different temperatures under a dry air (78% N_2 and 22% O_2) gas flow.

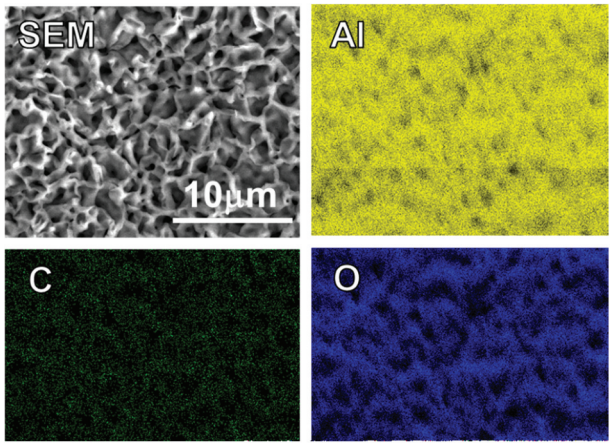

Figure 10. SEM micrograph and EDS maps of sintered Al_3BC_3 sample heated at 1500°C for 1 h under dry air (78% N_2 and 22% O_2) gas flow.

$$Al_{18}B_4O_{33} \rightarrow 9Al_2O_3(s) + 2B_2O_3(g)$$

The oxidation of Al_3BC_3 progressed with increasing heat-treatment temperature, and the amounts of $Al_{18}B_4O_{33}$ and Al_2O_3 increased continuously as the temperature was increased to 1500°C. Figure 10 shows an SEM micrograph and EDS maps for the surface of the Al_3BC_3 sample heated at 1500°C for 1 h under air. The surface became rough because of oxidation accompanied by the volatilization of B_2O_3 and CO_2, and oxide phases were observed. Interestingly, this surface morphology differed substantially from the previously reported needlelike $Al_{18}B_4O_{33}$ particles formed on the surface of $Al_8B_4C_7$ [9]. During oxidation of $Al_8B_4C_7$, the excess Al and B caused the formation of $Al_4B_2O_9$ and more B_2O_3 between 700°C and 800°C, which may have led to the observed surface morphology.

A cross-sectional SEM micrograph and EDS maps of the Al_3BC_3 particles heated at 1200 and 1500°C for 20 h are presented in Figure 11. The $Al_{18}B_4O_{33}$ formed on the surface of Al_3BC_3 undergoes further thermal decomposition. Extending the heating time led to oxidation not only at the surface of the Al_3BC_3 particles but also in their interior, resulting in monophasic Al_2O_3. We found that the $Al_{18}B_4O_{33}$ layer formed on the Al_3BC_3 surface did not inhibit oxidation and was completely oxidized when the sample was exposed to a high temperature in ambient air for a long period. Thus, Al_3BC_3 is expected to function as a structural component at temperatures as high as 1200°C; at temperatures greater than 1200°C, it appears to be suitable as an antioxidant for high-temperature structural ceramics such as ZrB_2, SiC, and SiC fiber-reinforced SiC (SiC_f/SiC) composites. Furthermore, since the CTE of Al_3BC_3 is between that of SiC_f (4.5×10^{-6}/°C) and Al_2O_3 (8.5×10^{-6}/°C), it is expected to be used instead of mullite, which is the interface between SiC_f/Al_2O_3 composite.

4. Conclusions

We measured various high-temperature properties of monophasic Al_3BC_3 and clarified its thermal shock resistance. The CTE for the unit cell was most anisotropic when Al_3BC_3 was heated to 500°C: the CTE along the *a*-axis was approximately twice that along the *c*-axis. Among the thermal expansion characteristics, CAl_5 trigonal bipyramids interleaved by short linear C – B – C units were found to be distorted at 400–600°C. A relative density of 96% was achieved by

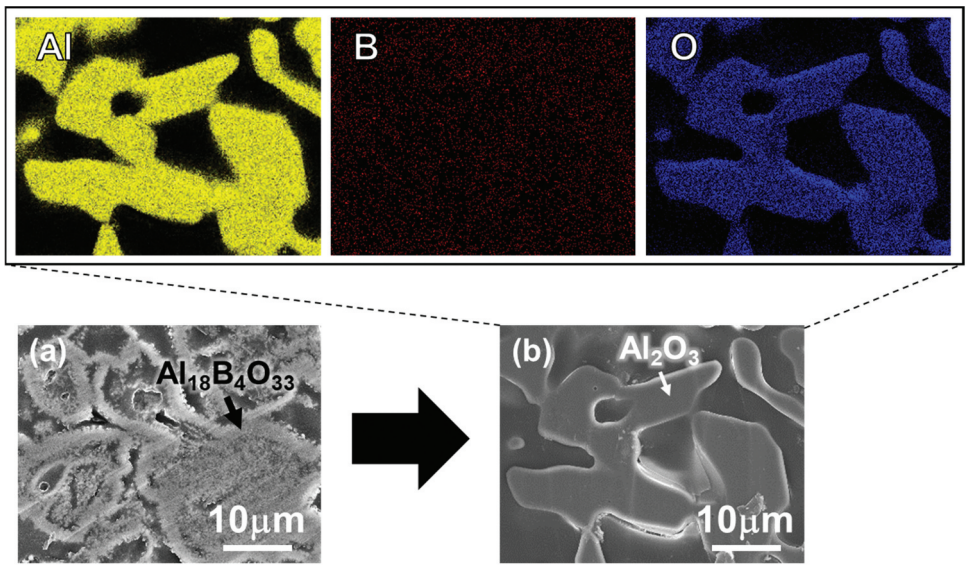

Figure 11. Cross-sectional SEM micrograph and EDS maps of Al_3BC_3 particles heated at (a) 1200°C and (b) 1500°C for 20 h under ambient air.

heating Al_3BC_3 powder at 1600°C under a uniaxial pressure of 40 MPa by SPS. The bending strength was 226 MPa at RT, which was lower than that previously reported for $Al_8B_4C_7$; this difference is attributed to the difficulty associated with densification without gas-phase diffusion via Al- and B-based gases or liquids. Al_3BC_3 exhibited a good thermal shock fracture resistance parameter R' of 3.3, which was equivalent to that for Al_2O_3 and substantially greater than those for Al_4SiC_4 and $Al_6Si_2O_{13}$, mainly because of the higher thermal conductivity and lower elastic modulus of Al_3BC_3. The dense Al_3BC_3 sample showed excellent thermal stability under N_2 and inert gas atmospheres but was easily oxidized to monophasic Al_2O_3 at 1300°C under ambient air. Thus, Al_3BC_3 is expected to be useful as a structural component at temperatures as high as 1200°C and to be suitable as an antioxidant for high-temperature structural ceramics at temperatures greater than 1200°C.

Acknowledgment

The authors thank the HT-XRD measurement using a fully automatic multi-purpose X-ray diffractometer (SmartLab, Rigaku, Japan).

Disclosure statement

No potential conflict of interest was reported by the author(s).

Funding

This study was supported by a research grant from The Technical Association of Refractories, Japan (TARJ).

ORCID

Ryosuke Maki http://orcid.org/0000-0002-0344-4470
Yoshihiro Kusano http://orcid.org/0000-0003-3646-3413

References

[1] Hashimoto S, Ishihara T, Inoue K, et al. Synthesis and mechanical properties of $Al_8B_4C_7$. J Ceram Soc Jpn. 2009;117(1361):18–21. doi: 10.2109/jcersj2.117.18
[2] Lee S-H. Low temperature pressureless sintering of SiC using an aluminum borocarbides additive. J Am Ceram Soc. 2011;94(9):2746–2748. doi: 10.1111/j.1551-2916.2011.04688.x
[3] Inoue Z, Tanaka H, Inomata Y. Synthesis and X-ray crystallography of aluminum boron carbide, $Al_8B_4C_7$. J Mater Sci. 1980;15(12):3036–3040. doi: 10.1007/BF00550372
[4] Hillebrecht H, Mayer FD. Synthesis, structure, and vibrational spectra of Al_3BC_3, a carbidecarboborate of aluminum with linear $(C=B=C)^{5-}$ anions. Angew Chem Int Ed Engl. 1996;35(21):2499–2500. doi: 10.1002/anie.199624991
[5] Lee S-H, Kim H-D, Choi S-C, et al. Chemical composition and microstructure of Al_3BC_3 prepared by different densification methods. J Eur Ceram Soc. 2010;30(4):1015–1020. doi: 10.1016/j.jeurceramsoc.2009.09.027
[6] Wang T, Yamaguchi A. Some properties of sintered $Al_8B_4C_7$. J Mater Sci Lett. 2000;19(12):1045–1046. doi: 10.1023/A:1006791004355
[7] Li F, Zhou Y, He L, et al. Synthesis, microstructure, and mechanical properties of Al_3BC_3. J Am Ceram Soc. 2008;91(7):2343–2348. doi: 10.1111/j.1551-2916.2008.02437.x
[8] Wang J, Zhou Y, Liao T, et al. First-principles prediction of low shear-strain resistance of Al_3BC_3: a metal borocarbide containing short linear BC_2 units. Appl Phys Lett. 2006;89(2):021917. doi: 10.1063/1.2220549
[9] Wang T, Yamaguchi A. Synthesis of $Al_8B_4C_7$ and its oxidation properties in air. J Ceram Soc Jpn. 2000;108(1256):375–380. doi: 10.2109/jcersj.108.1256_375
[10] Lee S-H, Tanaka H. Thermal stability of Al_3BC_3. J Am Ceram Soc. 2009;92(9):2172–2174. doi: 10.1111/j.1551-2916.2009.03171.x
[11] Wang T, Yamaguchi A. Antioxidation behavior and effect of $Al_8B_4C_7$ added to carbon-containing refractories. J Ceram Soc Jpn. 2000;108(1261):818–822. doi: 10.2109/jcersj.108.1261_818
[12] Chen Z, Zhao X, Wang H, et al. Preparation and properties of dense ZrB_2 composite reinforced by elongated SiC and Al_3BC_3 grains. Int J Appl Ceram Technol. 2019;16(6):2190–2196. doi: 10.1111/ijac.13265
[13] Zhao X, Chen Z, Wang H, et al. The influence of additive and temperature on thermal shock resistance of ZrB_2 based composites fabricated by spark plasma sintering. Mater Chem Phys. 2019;240:122061. doi: 10.1016/j.matchemphys.2019.122061
[14] Maki RSS, Matsumura S, Kida S, et al. Synthesis of monophasic Al_3BC_3 powder with hexagonal plate-like morphology. Inorg Chem. 2022;61(8):3493–3497. doi: 10.1021/acs.inorgchem.1c03424
[15] Bayer G. Thermal expansion characteristics and stability of pseudobrookite-type compounds, Me_3O_5. J Less-Common Met. 1971;24(2):129–138. doi: 10.1016/0022-5088(71)90091-9
[16] Kuscer D, Bantan I, Hrovat M, et al. The microstructure, coefficient of thermal expansion and flexural strength of cordierite ceramics prepared from alumina with different particle sizes. J Euro Ceram Soc. 2017;37(2):739–746. doi: 10.1016/j.jeurceramsoc.2016.08.032
[17] Momma K, Izumi F. VESTA 3 for three-dimensional visualization of crystal, volumetric and morphology data. J Appl Crystallogr. 2011;44(6):1272–1276. doi: 10.1107/S0021889811038970
[18] Francl J, Kingery WD. Thermal conductivity: iX, experimental investigation of effect of porosity on thermal conductivity. J Am Ceram Soc. 1954;37(2):99–107. doi: 10.1111/j.1551-2916.1954.tb20108.x
[19] Inoue K, Mori S, Yamaguchi A. Thermal conductivity and temperature dependence of linear thermal expansion coefficient of Al_4SiC_4 sintered borides prepared by pulse electronic current sintering. J Ceram Soc Jpn. 2003;111(1293):348–351. doi: 10.2109/jcersj.111.348
[20] Liu J, Zhou X, Tatarko P, et al. Fabrication, microstructure, and properties of SiC/Al_4SiC_4 multiphase ceramics via an in-situ formed liquid phase sintering. J Adv Ceram. 2020;9(2):193–203. doi: 10.1007/s40145-020-0359-8
[21] Taira H, Nishikawa T, Hoshiyama Y, et al. (Properties and applications of Al_4SiC_4) Al_4SiC_4 no tokusei to ouyou (in Japanese). In: Mizota Y, editor. Okayama,

Japan: Okayama Ceramics Research Foundation; 2019. p. 69–72.
[22] Sun L, Gao Y, Li Y, et al. Structural, bonding, anisotropic mechanical and thermal properties of Al_4SiC_4 and $Al_4Si_2C_5$ by first-principles investigations. J Asian Ceram Soc. 2016;4(3):289–298. doi: 10.1016/j.jascer.2016.05.006
[23] Santana LNL, Gomes J, Neves GA, et al. Mullite formation from bentonites containing kaolinite: effect of composition and synthesis parameters. Appl Clay Sci. 2014;87:28–33. doi: 10.1016/j.clay.2013.11.018
[24] Rajaei H, Mobasherpour I, Farvizi M, et al. Effect of mullite synthesis methods on the spark plasma sintering behaviour and mechanical properties. Micro Nano Lett. 2016;11(8):465–468. doi: 10.1049/mnl.2016.0092
[25] Brunauer G, Frey F, Boysen H, et al. High temperature thermal expansion of mullite: an in situ neutron diffraction study up to 1600°C. J Euro Ceram Soc. 2001;21(14):2563–2567. doi: 10.1016/S0955-2219(01)00267-9
[26] Mahnicka-Goremikina L, Svinka R, Svinka V, et al. Thermal properties of porous mullite ceramics modified with microsized ZrO_2 and WO_3. Materials. 2022;15(22):7935. doi: 10.3390/ma15227935
[27] Ružić J, Maletaškić J, Radovanović Ž, et al. Mechanical properties of mullite investigated by nanoindentation. Metal Mater Data. 2024;2(2):47–50. doi: 10.30544/MMD29
[28] Kakroudi MG, Vafa NP, Asl MS, et al. Effects of SiC content on thermal shock behavior and elastic modulus of cordierite–mullite composites. Ceram Int. 2020;46(15):23780–23784. doi: 10.1016/j.ceramint.2020.06.153
[29] Hasselman DPH. Thermal stress resistance parameters for brittle refractory ceramics: a compendium. Am Ceram Soc Bull. 1970;49:1033–1037.
[30] Yu C, Xing G, Ke L, et al. Thermal stability of Al_3BC_3 powders under a nitrogen atmosphere. Int J Mater Res. 2023;114(12):1138–1145. doi: 10.1515/ijmr-2022-0347